JGR Atmospheres

RESEARCH ARTICLE
10.1029/2022JD036767

Cooling and Contraction of the Mesosphere and Lower Thermosphere From 2002 to 2021

Martin G. Mlynczak[1], Linda A. Hunt[2], Rolando R. Garcia[3], V. Lynn Harvey[4], Benjamin T. Marshall[5], Jia Yue[6], Christopher J. Mertens[1], and James M. Russell III[7]

[1]NASA Langley Research Center, Hampton, VA, USA, [2]SSAI, Hampton, VA, USA, [3]National Center for Atmospheric Research, Boulder, CO, USA, [4]Laboratory for Atmospheric and Space Physics, University of Colorado, Boulder, CO, USA, [5]GATS, Inc., Newport News, VA, USA, [6]Catholic University of America/NASA Goddard Space Flight Center, Greenbelt, MD, USA, [7]Hampton University, Hampton, VA, USA

Key Points:

- Satellite measurements of temperature, geopotential height, and thickness reveal a cooling, contracting mesosphere and lower thermosphere (MLT)
- MLT temperatures in the two recent solar minima (2008–2009 and 2019–2020) were likely the coldest since the start of the Industrial Age
- Cold temperatures at 10^{-4} hPa in 2019 may be the result of lower solar irradiance in the Schumann–Runge bands (175–200 nm)

Correspondence to:

M. G. Mlynczak,
m.g.mlynczak@nasa.gov

Citation:

Mlynczak, M. G., Hunt, L. A., Garcia, R. R., Harvey, V. L., Marshall, B. T., Yue, J., et al. (2022). Cooling and contraction of the mesosphere and lower thermosphere from 2002 to 2021. *Journal of Geophysical Research: Atmospheres*, *127*, e2022JD036767. https://doi.org/10.1029/2022JD036767

Received 22 MAR 2022
Accepted 22 SEP 2022

Author Contributions:

Conceptualization: Martin G. Mlynczak
Formal analysis: Martin G. Mlynczak, Linda A. Hunt, Rolando R. Garcia, V. Lynn Harvey, Benjamin T. Marshall, Jia Yue
Methodology: Martin G. Mlynczak, Linda A. Hunt, Rolando R. Garcia, Christopher J. Mertens
Resources: Martin G. Mlynczak
Validation: Rolando R. Garcia
Visualization: Linda A. Hunt, Jia Yue
Writing – original draft: Martin G. Mlynczak

Abstract We examine the thermal structure of the mesosphere and lower thermosphere (MLT) using observations from 2002 through 2021 from the SABER instrument on the NASA TIMED satellite. These observations show that the MLT has significantly cooled and contracted between the years 2002 and 2019 (the year of the most recent solar minimum) due to a combination of a decline in the intensity of the 11-year solar cycle and increasing carbon dioxide (CO_2.) During this time the thickness of atmosphere between the 1 and 10^{-4} hPa pressure surfaces (approximately 48 and 105 km) has contracted by 1,333 m, of which 342 m is attributed to increasing CO_2. All other pressure surfaces in the MLT have similarly contracted. We further postulate that the MLT in the two most recent solar minima (2008–2009 and 2019–2020) was very likely the coldest and thinnest since the beginning of the Industrial Age. The sensitivity of the MLT to a doubling of CO_2 is shown to be −7.5 K based on observed trends in temperature and growth rates of CO_2. Colder temperatures observed at 10^{-4} hPa in 2019 than in the prior solar minimum in 2009 may be due to a decrease of 5% in solar irradiance in the Schumann-Runge band spectral region (175–200 nm).

Plain Language Summary The region of the atmosphere from 48 to 105 km (30 miles to 65 miles) above the Earth's surface is called the mesosphere and lower thermosphere or MLT. In this paper we show that the MLT has cooled dramatically from the year 2002–2019, by as much as 1.75 to 19 K (3.1–34.2 degrees Fahrenheit), depending on altitude. These results are obtained from temperatures measured by an instrument on a satellite in low Earth orbit since 2002. The observed cooling is attributed to a reduction in solar activity that influences the MLT temperature and to an increase of carbon dioxide (CO_2) in the MLT. The observed cooling of the MLT due to increasing CO_2 is an expected result. Between 2002 and 2019 the MLT contracted or shrank by up to 1,333 m or over 4,700 feet. A total of 342 m (1,142 feet) of this shrinkage is attributed to increasing CO_2 and is considered a permanent change to the atmosphere. Our results also show that the MLT is expected to cool by 7.5 K (13.5 degrees Fahrenheit) due to a doubling of CO_2 which is a benchmark calculation often used for comparison with other results.

1. Introduction

"Since carbon dioxide (CO_2) plays a significant role in the heat budget of the atmosphere, it is reasonable to suppose that continued increases would affect climate." With these words, the late Verner Suomi eloquently stated the hypothesis of climate change science in 1979, in his foreword to the seminal "Charney Report" (National Research Council, 1979) on the role of CO_2 and climate. The remarkable prescience of the Charney Report was noted upon its 40th anniversary (Nicholls, 2019). Specifically, the scientists who developed the report under the direction of the late Jule Charney predicted that, for a doubling of CO_2 in Earth's atmosphere, the Earth's surface air temperature would warm by approximately 3 C, with a probable error of 1.5 C. Prior to the Charney report, Sawyer (1972) made the case for a warming troposphere due to increasing CO_2 and presciently predicted 0.6 K warming by the year 2000. Remarkably, the most recent assessment of Earth's equilibrium climate sensitivity (ECS) (i.e., the average global surface air temperature change after a doubling CO_2) (Sherwood et al., 2020) sets its bounds between 2.3 and 4.5 C, nearly identical to the Charney report range.

Verner Suomi's hypothesis statement, "carbon dioxide plays a significant role in the heat budget of the atmosphere" is true throughout the entire perceptible atmosphere from Earth's surface to the edge of space. It has long

Writing – review & editing: James M. Russell

been known that infrared radiation from CO_2 (and ozone and water vapor) in the stratosphere, mesosphere, and lower thermosphere (to about 130 km altitude) work to balance the (largely ultraviolet) energy from the Sun absorbed in these regions by ozone and molecular oxygen (Curtis & Goody, 1956; Dickinson, 1984; Kuhn & London, 1969; London, 1980; Mertens et al., 1999; Mlynczak, Hunt, et al., 2018; Mlynczak et al., 1999, 2010; Roble & Dickinson, 1989). Infrared radiation from nitric oxide (Kockarts, 1980; Mlynczak, Hunt, et al., 2021) and the two fine structure lines of atomic oxygen (Bates, 1951), in addition to that from CO_2, are key components of the energy budget of the middle and upper thermosphere. Heat conduction also removes energy from the middle and upper thermosphere by transporting heat downward into the lower thermosphere where it is radiated by CO_2 in the "heat sink" region (Mlynczak, Knipp, et al., 2018) between 90 and 135 km. Thus, to paraphrase Suomi, it is reasonable to suppose that increasing CO_2 will have an impact on the climate of the stratosphere, mesosphere, and thermosphere as well. More specifically, since the effect of CO_2 is to cool the upper atmosphere, it is expected that a decline in the temperature of the upper atmosphere would be observed in time as CO_2 increases (Cicerone, 1990; Roble & Dickinson, 1989). Indeed, this cooling has been observed over the past 40 years, from the stratosphere and extending up into the geospace environment at altitudes of low-Earth orbiting satellites (Emmert, 2015; Garcia et al., 2019; Randel et al., 2017; Zhao et al., 2021). In addition, Garcia et al. (2019) also showed good agreement between observed trends and modeled trends, within the measurement and model uncertainties. Trends derived by Zhao et al. (2021) and by Garcia et al. (2019) using SABER data show a general agreement. However, Zhao et al. (2021) derived trends at fixed altitudes while Garcia et al. (2019) derived trends on pressure surfaces, as we also do in this paper. The results of Zhao et al. (2021) cannot be directly compared with those of Garcia et al. (2019) or with those presented herein because trends at fixed altitudes will be impacted by the contracting of the atmosphere, which we show to be significant. The temperature trends derived in the present work will be shown to be consistent with Garcia et al. (2019) on common pressure surfaces.

The purpose of this paper is to examine trends in temperature, geopotential height (GPH), and thickness of layers in the atmosphere between 1 and 10^{-4} hPa between 2002 and 2021. We also ascribe the causes of these changes and trends to increasing CO_2 and to the progressively weaker solar cycle during this time. Recent minima in temperature in the mesosphere and lower thermosphere (MLT) are placed in historical context, considering the buildup of CO_2 since the beginning of the Industrial Age. Conditions induced by the solar cycle are expected to be cyclical while the long-term trend of the MLT temperature is toward a permanently colder state. We further show how the derived trends can place a boundary on the sensitivity of the MLT to doubled CO_2. These observations, coupled with analysis of the CO_2 concentration and solar activity over the past several hundred years lead to the conclusions that (a) the MLT is cooling and contracting, and (b) the MLT in the two recent solar minima, 2008–2009 and 2019–2020, was very likely the coldest and thinnest since the beginning of the Industrial Age due to the combination of low solar activity and increasing CO_2.

In Section 2 we present the methodology used to analyze the SABER observations of temperature, GPH, and thickness from January 2002 through December 2021. These are evaluated considering the observed solar activity and observed increases in CO_2 over the last 20 years. In Section 3 we examine the growth rate of CO_2 and propose hypotheses on MLT temperatures extending back to the beginning of the Industrial Age. In Section 4 we examine radiative relaxation times and derive the sensitivity of the MLT temperature to a doubling of CO_2. In Section 5 we examine and discuss uncertainties in SABER data and the analyses and possible implications for the results presented herein. A summary in Section 6 concludes the paper.

2. Methodology

The SABER instrument on the TIMED satellite has been deriving vertical temperature and GPH profiles in the MLT since January 2002. Remsberg et al. (2008) and (Garcia-Comas et al., 2008) provide an assessment of SABER temperature quality, which is discussed further in Section 5. Remsberg et al. (2008) also discuss the derivation of GPH.

In this paper we use SABER Version 2.07 and 2.08 temperature and GPH data. These data are available for both day and night continuously. For the retrieval of SABER temperature in these versions, the required CO_2 concentration is provided by the Whole Atmosphere Community Climate Model (WACCM) (Gettelman et al., 2019). We begin by computing daily global averages of temperature and GPH on the 1, 10^{-1}, 10^{-2}, 10^{-3}, and 10^{-4} hPa pressure surfaces from January 2002 through December 2021. (These data, comprised of over 7,200 points per time series, are shown in Figures 1–3). The separation in pressure surfaces by a factor of 10 is to facilitate the

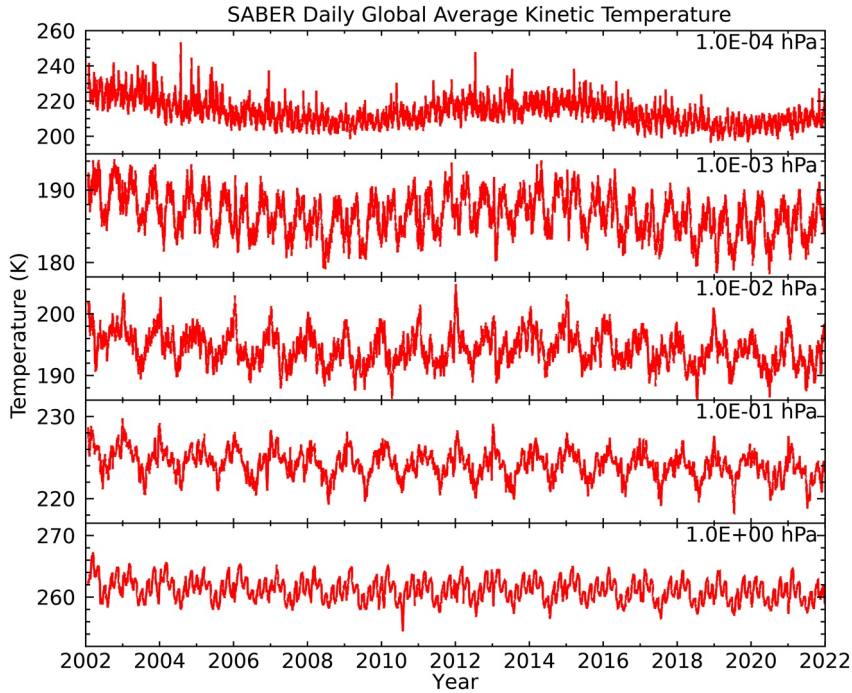

Figure 1. Daily global average (55°N to 55°S) temperature (K) at five different pressure levels from January 2002 through December 2021. More than 7,200 days of data are plotted for each pressure level.

assessment of the contraction of the atmosphere throughout the MLT. The range in pressures cover atmospheric regions from the lower boundary of the mesosphere (as we define it for this paper) into the lower thermosphere over an approximate altitude range of 48–105 km. We define the thickness as the difference in GPH between two

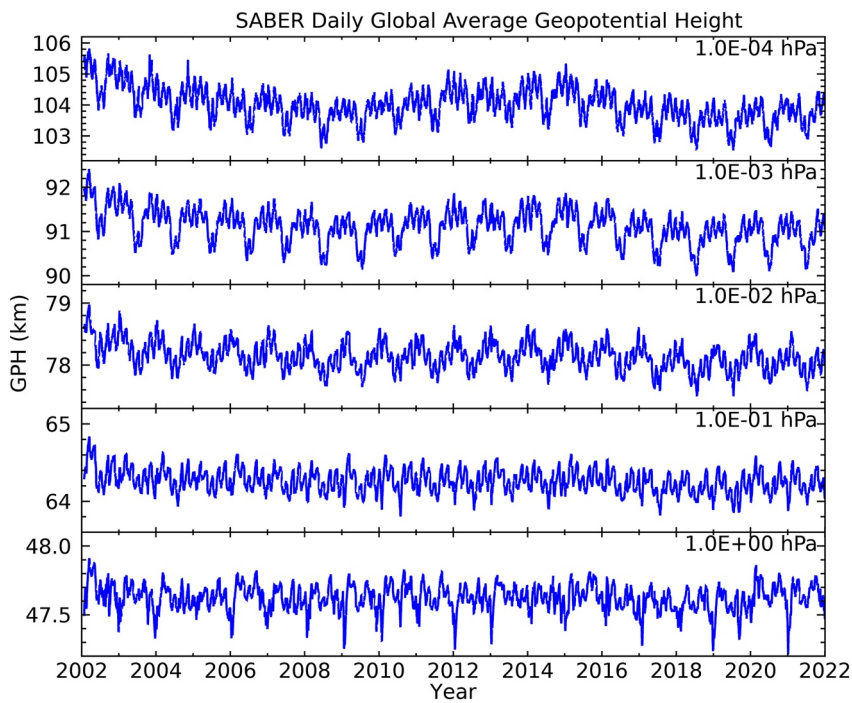

Figure 2. Daily global average (55°N to 55°S) geopotential height (GPH, m) at five different pressure levels from January 2002 through December 2021. More than 7,200 days of data are plotted for each pressure level.

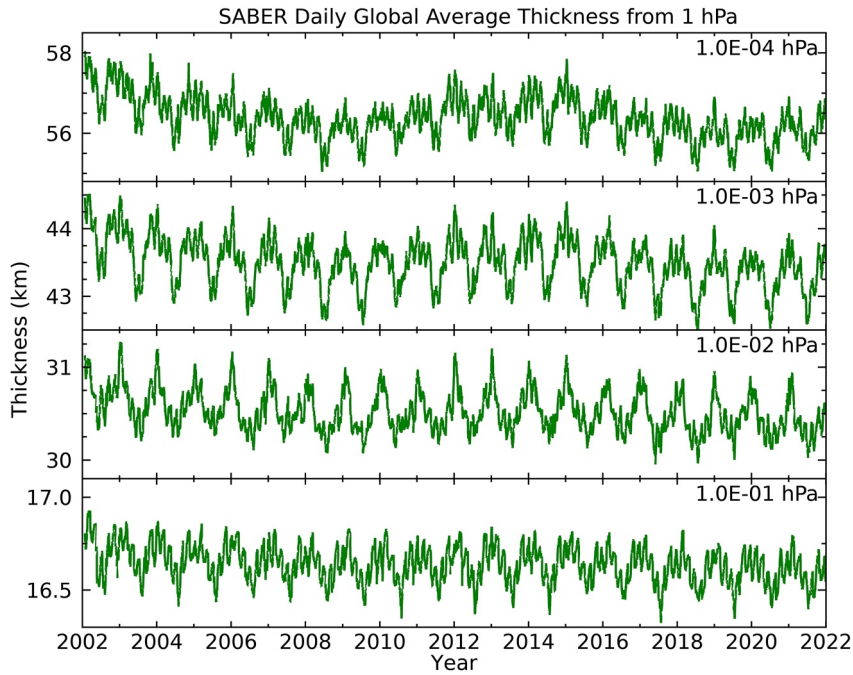

Figure 3. Daily global average (55°N to 55°S) thickness (m) at five different pressure levels from January 2002 through December 2021. More than 7,200 days of data are plotted for each pressure level.

pressure surfaces. Changes in this difference reflect the expansion and contraction of the atmosphere between the respective pressure surfaces.

The following metrics related to long-term changes are assessed in this paper: changes in temperature, GPH, and thickness and attribution of those changes to the declining strength of the solar cycle and to the increase in CO_2 over the past two decades. Trends and attributions are attained by first computing global annual means of temperature and GPH for the 20-year time span 2002 through 2021 from the time series in Figures 1–3. Here "global" is defined as the region between ±55° in latitude that SABER observes continuously. The global annual mean thickness is computed relative to the 1 hPa surface for the remaining four surfaces by differencing the respective global annual mean geopotential heights. The TIMED satellite orbit is such that all local times are sampled every 60 days. The movement of the Sun relative to the spacecraft over this time requires the spacecraft to conduct a "yaw" maneuver that rotates the spacecraft 180° to keep SABER and its thermal radiator pointed away from the Sun. We therefore define an annual mean to encompass six consecutive yaw cycles (360 days). Year 1 begins on 22 January 2002 and Year 20 ends on 20 December 2021. This averaging approach removes the effects of tides (diurnal and semidiurnal variations of temperature) on the resulting time series. These annual mean data are shown in Figure 4.

The GPH and temperature time series are screened for anomalous values. The GPH data were screened to check whether the values at a given pressure level were more than ±5 km from the mean of the values at that pressure level. Those values were considered outliers since most values (99.3%) are with ± 1 km of the mean. A total of 48 days out of the 7,281 days in the time series contained anomalous values and are removed from the daily global mean GPH time series on all pressure surfaces. These same 48 days are also removed from the daily global mean temperature time series and were found to eliminate all the anomalous temperature values as well.

To compute trends and attribute changes to temperature, GPH, and thickness, multiple linear regression (MLR) is applied to the 14 global annual time series (five temperature time series, five GPH time series, and four thickness time series). The regression is of the form $G = a + b \times \mathrm{F10.7} + c \times t$, where G is the quantity temperature, GPH, or thickness, F10.7 is the annual average of the F10.7 solar radio flux index, and t is time. The slope "c" is the trend in the quantity computed in a time unit of per year. We note Garcia et al. (2019) included in their MLR two terms related to the quasi-biennial oscillation and one term for stratospheric aerosol in addition to F10.7 and time.

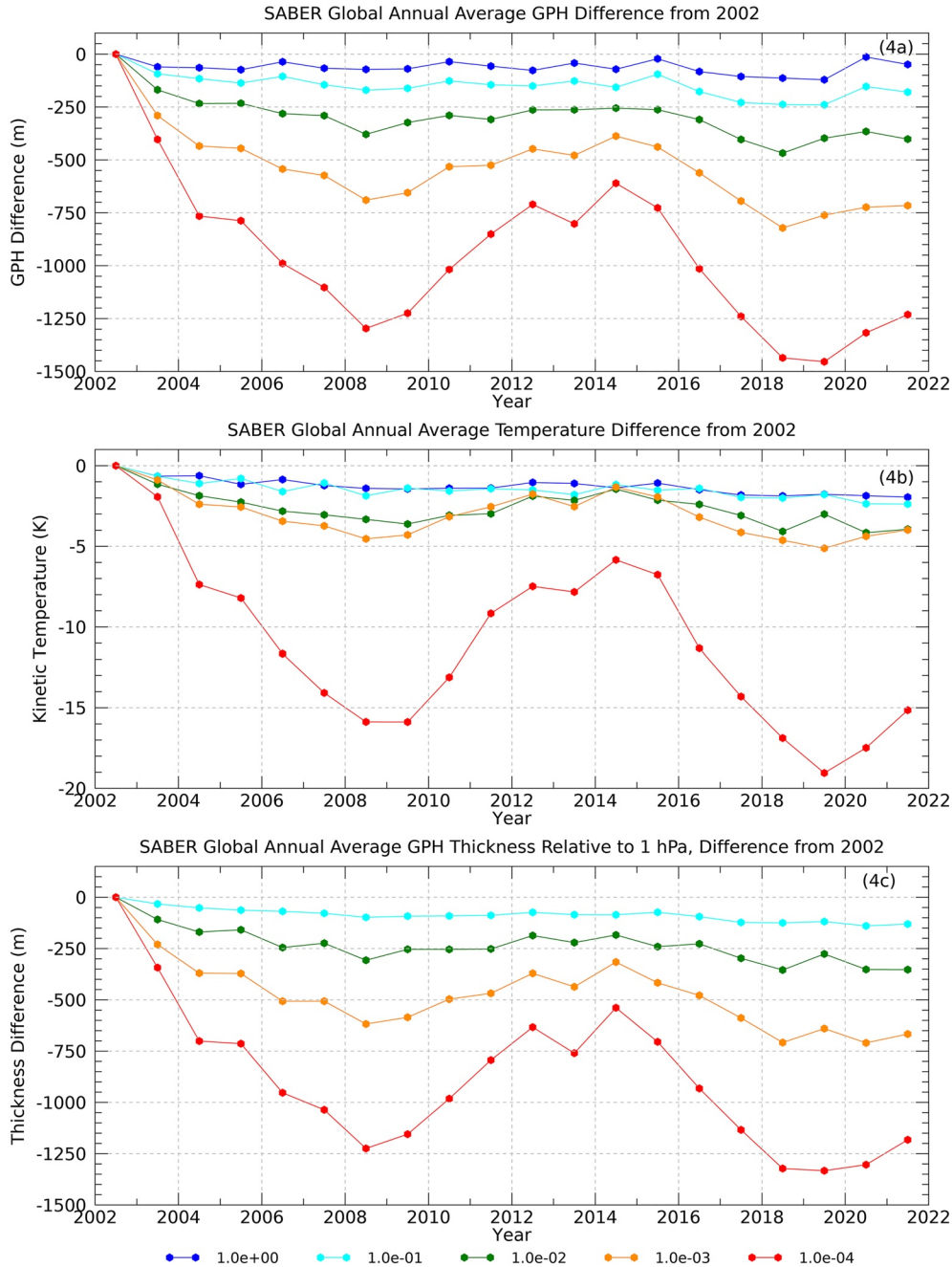

Figure 4. (a) Change in the global annual mean geopotential height (GPH, m) from the year 2002 on the five pressure levels indicated in the color code underneath Figure 2c. (b) Change in global annual mean temperature (K) from the year 2002 on the five indicated pressure levels. (c) Change in global annual mean thickness (m) from 2002 for the four pressure levels indicated. The thickness is defined as the difference between the global annual mean GPH on the indicated pressure level and the global annual mean GPH at 1 hPa.

These parameters did not significantly influence their derived trends and so we do not consider these or other terms in the MLR results presented here.

We report the attribution of the observed changes from 2002 to 2019 as solar minimum occurred in late 2019. The change in *T*, GPH, or thickness due to increasing CO_2 is taken to be the trend value ("*c*") multiplied by 18 years. The change due to weakening of the solar cycle since 2002 is taken as the difference between the observed total

Table 1
Observed Changes From 2002 to 2019 in Global Annual Mean Temperature, Geopotential Height (GPH), and Thickness (Relative to 1 hPa) (Obs. Change); the Trend in Each Quantity Due To Increasing CO_2 (Derived Trend); the Estimated Magnitude of the Change in Each Quantity Due To Increasing CO_2 (Δ CO_2); and the Estimated Magnitude of the Change in Each Quantity Due To Declining Solar Activity (Δ Solar)

Quantity	P (hPa)	Obs. Change	Derived trend	Δ CO_2	Δ Solar
Temperature	1	−1.77 K	−0.55 ± 0.07 K/dec	−0.99 K	−0.78 K
	10^{-1}	−2.05 K	−0.63 ± 0.11 K/dec	−1.13 K	−0.92 K
	10^{-2}	−3.01 K	−0.53 ± 0.17 K/dec	−0.95 K	−2.06 K
	10^{-3}	−5.12 K	−0.51 ± 0.17 K/dec	−0.92 K	−4.20 K
	10^{-4}	−19.05 K	−2.60 ± 0.67 K/dec	−4.68 K	−14.37 K
GPH	1	−121 m	−8 ± 12.3 m/dec	−14.4 m	−106.6 m
	10^{-1}	−240 m	−47 ± 12.9 m/dec	−84.6 m	−155.4 m
	10^{-2}	−397 m	−84 ± 14.9 m/dec	−151.2 m	−245.8 m
	10^{-3}	−761 m	−127 ± 20.0 m/dec	−228.6 m	−532.4 m
	10^{-4}	−1,454 m	−197 ± 33.6 m/dec	−354.6 m	−1,099.4 m
Thickness	10^{-1}	−118 m	−40 ± 3.7 m/dec	−72 m	−46 m
	10^{-2}	−276 m	−77 ± 13.4 m/dec	−138.6 m	−137.4 m
	10^{-3}	−640 m	−119 ± 18.5 m/dec	−214.2 m	−425.8 m
	10^{-4}	−1,333 m	−190 ± 31.6 m/dec	−342 m	−991 m

Note. One-sigma trend uncertainties are also listed in the derived trend column.

change between 2002 and 2019 and the computed change due to increasing CO_2. These results are shown in Table 1.

2.1. SABER Observations of MLT Temperature, Geopotential Height, and Thickness Changes From 2002 to 2019/2020

The daily global average time series of temperature, GPH, and thickness are shown in Figures 1–3 on the pressure levels as indicated. Substantial variability is visually evident on many time scales. In Figure 1 and on the 10^{-1} hPa surface, a clear annual cycle in temperature is evident while at 10^{-3} hPa a semi-annual cycle is evident. The 11-year solar cycle is visually evident on the 10^{-4} hPa surface. The variability in GPH shown in Figure 2 is markedly different than temperature. A strong annual cycle is visually evident in GPH at 10^{-2}, 10^{-3}, and 10^{-4} hPa while the 11-year solar cycle is visually evident at 10^{-3} and 10^{-4} hPa. The time series of thickness (difference in GPH of indicated pressure level and the GPH at the 1 hPa level) in Figure 3 indicates a strong annual cycle for all four layers of the MLT. In addition, the 11-year solar cycle is evident in the layers at 10^{-4} and 10^{-3} hPa.

Figure 4 shows time series on each pressure surface of the global annual mean *T*, GPH, and thickness (relative to the 1 hPa surface) computed from the daily global mean time series in Figures 1–3. Since we are most interested in changes of the three quantities, the values plotted in Figure 4 are the *difference* in each quantity from its value in 2002. We will discuss differences relative to 2019 as the most recent solar minimum occurred in December 2019.

The first obvious result is that thickness (Figure 4c) of the four layers defined by their respective pressure levels is less in 2019 and 2020 than in 2002, implying a contraction or cooling of the entire MLT over that time. Three of the four layers exhibit evidence of the 11-year solar cycle in their time series. The overall trend is toward "thinner" layers of the MLT. Attribution of the thinning will be addressed in Section 3. The increase in thickness at 10^{-4} and 10^{-3} hPa after 2019 is evidence of increasing solar activity with the onset of solar cycle 25.

Similarly, GPH is observed to decrease from 2002 to 2019/2020 on all five pressure levels (Figure 4a). The observed decrease in GPH of the 1 hPa pressure surface (121 m in 2019, see Table 1) is indicative of a contracting stratosphere (Pisoft et al., 2021). The observed decrease in GPH from 2002 to 2019 is 1,454 m (see Table 1). The effects of the 11-year solar cycle are visually evident in the GPH time series in Figure 4a, particularly on

pressure levels of 0.01 hPa or less. This is expected as the effects of the solar cycle are more predominant due to the absorption of shorter wavelength and more variable (Coddington et al., 2016) ultraviolet radiation at higher altitudes (lower pressures).

Figure 4b shows the difference in global annual average temperature on the five pressure surfaces since 2002. All five pressure surfaces are colder in 2019 or 2020 than in 2002. The largest changes in temperature and evidence of the solar cycle occur on the 10^{-2}, 10^{-3}, and 10^{-4} pressure surfaces. These results, along with the GPH and thickness results, point to a cooling and contracting MLT from 2002 to 2019.

2.2. Attribution of Changes in Temperature, GPH, and Thickness

A key question regarding the observed changes shown in Figure 4 is "what are the relative roles of increasing CO_2 and of decreasing solar activity in producing these changes?" As noted above, we apply MLR against time and the F10.7 solar radio flux to the global annual average temperature, GPH, and thickness time series shown in Figure 4. The MLR provides a slope (linear change of a quantity with time) which is interpreted as the quantity rate of change due to increasing CO_2. The change in each quantity due to increasing CO_2 (Δ CO_2 in Table 1) is calculated from the product of the trend and a time span of 18 years (2002–2019, when the most recent solar minimum occurred). The change due to the declining solar cycle intensity (Δ Solar in Table 1) is computed from the total observed change and the change derived due to CO_2 increase.

Table 1 shows the results of these calculations. The three quantity names are listed in the left column, followed by the pressure levels (hPa). The column labeled "Obs. Change" is the difference from 2002 to 2019 in the global annual mean value of each quantity, on each indicated pressure surface. The Derived Trend column is the trend in K/decade or m/decade computed from the linear regression process along with the corresponding one-sigma uncertainty in the trend. The trends and uncertainties are derived using the REGRESS routine in the IDL programming language. The results show a cooling and contracting mesosphere between 2002 and 2019. The trends and trend uncertainties in temperature between 1 and 10^{-3} hPa are consistent with the those derived by Garcia et al. (2019).

Table 1 also shows GPH decreases ranging from 121 to 1,454 m between 1 hPa and 10^{-4} hPa while the thickness of the atmosphere layers relative to 1 hPa has decreased by 118–1,333 m. Overall the decreases in each quantity due to increasing CO_2 and solar cycle intensity decrease are comparable at pressures greater than or equal to 10^{-1} hPa. At lower pressures the decline in solar cycle intensity is responsible for more of the observed changes. At 10^{-4} hPa the declining solar cycle is responsible for a cooling of as much as 14.37 K (out of a change of more than 19 K), a decrease in GPH of 1,099.4 m, and a decrease in thickness of 991 m.

The derived trend in temperature of 2.6 K per decade (with a computed trend uncertainty of 0.67 K/decade) at 10^{-4} hPa attributed in Table 1 to CO_2 increase is substantially larger than the trends at lower altitudes. Garcia et al. (2019) did not evaluate trends at 10^{-4} hPa so it is not possible to compare this result with their calculations. However, it will be shown in the upcoming discussion on sensitivity of the MLT to increasing CO_2 that a 2.6 K per decade trend is likely non-physical due to the large sensitivity in temperature to a doubling of CO_2 it implies. In addition, the trend is four to five times larger than on the other four pressure levels. Figure 4b also shows that the 10^{-4} hPa pressure surface is 3 K colder during the most recent solar minimum in 2019 than in the prior solar minimum from 2008 to 2009, which itself is often described as a "deep" minimum. These results raise two questions: (a) is the SABER temperature trend at 10^{-4} hPa correct and (b) what is the cause of the colder temperature at 10^{-4} hPa in 2019?

The lower thermosphere above 100 km is strongly heated through the absorption of solar ultraviolet radiation by molecular oxygen in the Schumann-Runge continuum (SRC) from 130 to 175 nm and in the Schumann-Runge Bands (SRB) from 175 to 200 nm. This critical spectral region is measured by the SEE instrument on the TIMED satellite (Woods et al., 2005) and by the SORCE satellite (Woods et al., 2022). We considered whether the solar irradiance was significantly lower during 2019–2020 than during the prior minimum from 2008 to 2009 as a possible mechanism to account for the colder SABER temperatures observed at 10^{-4} hPa in 2019 than 2008–2009. Woods et al. (2022), their Figure 14, show a statistically significant reduction of solar irradiance in the SRB measured by SORCE of as much as 6% from 2008 to 2009 to 2019–2020. This will reduce the heating rate in the lower thermosphere SRB by as much as 6%. Woods et al. (2022) also indicate a reduction in solar irradiance in the SRC of as much as 3% but it is not statistically significant. We suggest that the reduction of the solar

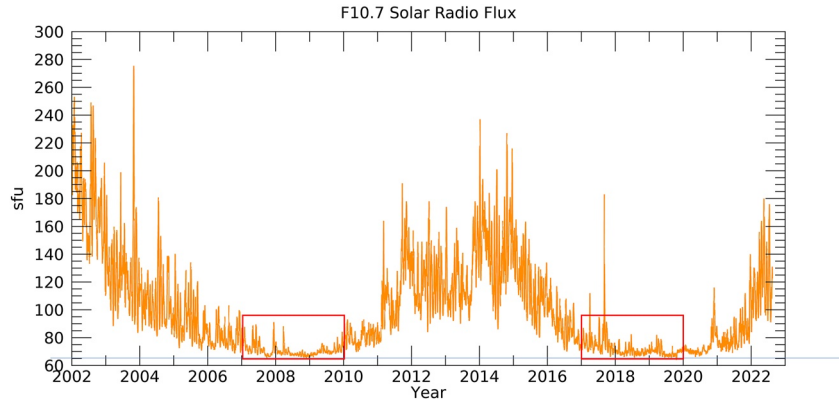

Figure 5. Daily F10.7 solar radio flux (1 sfu = 10^{-22} W m^{-2} Hz^{-1}) from January 2002 through July 2022. The red boxes indicate the years 2007–2010 and 2017–2020 around the two recent solar minima. F10.7 is not obviously lower in 2017–2020 than in 2007–2020.

irradiance in the SRB may be responsible for the colder observed temperatures in 2019 than in 2009 and that the effects of such a reduction on temperature be examined in a modeling study with the WACCM.

Figure 5 shows the daily F10.7 solar radio flux from 2002 to 2022. The 3-year periods surrounding the two most recent solar minima are highlighted by red boxes. F10.7 is not observed to be significantly less in magnitude in 2019–2020 than in 2008–2009. Therefore, the F10.7 index does not appear to replicate the observed decrease in solar irradiance in the SRB by the SORCE instrument and therefore may not be a reliable proxy for trend determination.

In summary, the SORCE results suggest two possible conclusions: (a) the decrease in observed SABER temperature at 10^{-4} hPa in 2019 may be associated with a decrease in the solar irradiance in the SRB, and (b) the F10.7 solar index does not correlate well with the observed decrease in the SRB irradiance nor with the observed decrease in temperature at 10^{-4} hPa, potentially making it unsuitable as a solar irradiance proxy for temperature trend analysis in the lower thermosphere. Further research is needed to confirm these conjectures.

3. Growth Rate of Mesospheric CO_2 and Hypotheses of Historical MLT Temperatures

CO_2 has been increasing in Earth's atmosphere since the start of the Industrial Age. Measurements in the MLT by the SABER instrument (Rezac et al., 2018; Yue et al., 2015) have shown that the concentration of CO_2 is increasing in the upper MLT (80 km and above) at a rate of 5%–6% per decade, similar to the rate measured at the Mauna Loa Observatory at Earth's surface. Figure 6 shows the growth of (global mean) MLT CO_2 from SABER (red curve), the observed growth of CO_2 measured at Earth's surface at the Mauna Loa, Hawaii, Observatory (blue curve), and CO_2 from ice core records dating from Antarctica dating back to the start of the Industrial Age (green curve) (Frank et al., 2010). The observed MLT growth rate of CO_2 is consistent with the record from Mauna Loa and with the record from the ice core. However, the CO_2 concentration (in ppm) in the MLT is less than at the surface due to the transport lifetime between the tropopause and 80 km and to the impact of diffusive separation which reduces the CO_2 volume mixing ratio above 80 km.

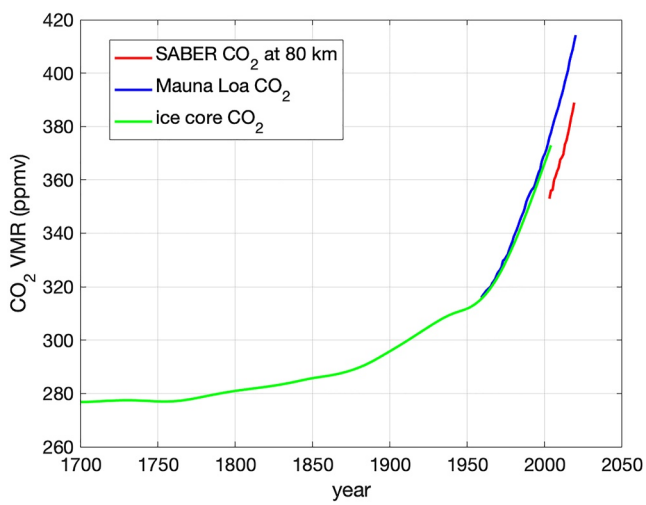

Figure 6. Observed CO_2 concentrations at the surface from the Mauna Loa Observatory in Hawaii (19.54°N, 155.58°W) (blue curve), from the ice core record (green curve), and in the mesosphere at 80 km from SABER (red curve). The growth rates are observed to be consistent among all three measurements.

The data in Figure 6 indicate that CO_2 at Earth's surface today is the largest in over 270 years. Due to the correspondence in observed growth rates over the last 20 years, we hypothesize that the MLT CO_2 is the highest now since the start of the Industrial Age and very likely as far back as 1,000 years or longer. This conclusion implies that the radiative cooling effects of CO_2 on

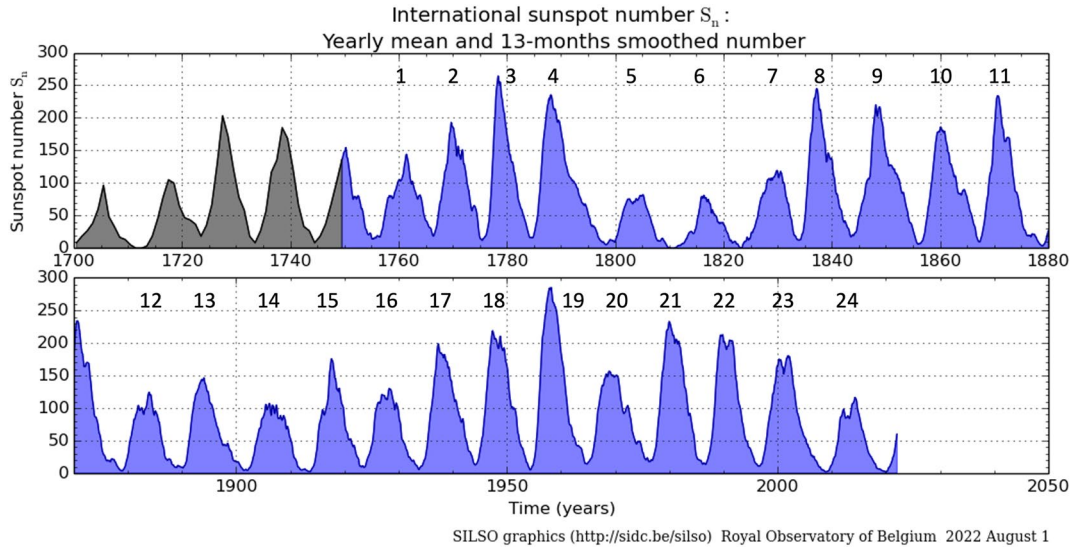

Figure 7. The International sunspot number since 1700. This figure is directly from the Sunspot Index and Long-Term Solar Observations (SILSO) website at the Royal Observatory of Belgium and was last updated on 1 August 2022. The data from 1700 to 1749 are the yearly average sunspot number (black shading). From 1749 to the present the data are the 13-month smoothed sunspot number [http://www.sidc.be/silso/yearlyssnplot]. The numbers above each cycle enumerate each complete solar cycle since the mid-1700s.

the temperature of the MLT are now larger than at any time since the beginning of the Industrial Age. We therefore postulate that the combined effects of increasing CO_2 and currently weak solar cycles make the two most recent MLT solar minimum temperatures the coldest since the start of the Industrial Age. Figure 7 illustrates the sunspot number since the start of the Industrial Age. The numerals above each cycle correspond to the sequence of each complete solar cycle since then. Apart from the solar cycles 5, 6, and 7 between 1800 and 1830, the solar cycles since 1750 are stronger than or comparable to the recently completed solar cycle 24. These three cycles between 1800 and 1830 are substantially weaker than SC 23 and slightly weaker than SC 24, implying slight cooling effects on the MLT at between 1800 and 1830 relative to today. However, the very low CO_2 abundance between 1800 and 1830 would still result in a net warmer MLT than is occurring today.

4. Sensitivity of the MLT to Increasing Carbon Dioxide

A key metric in defining the long-term effects of increasing CO_2 on surface temperature is the ECS. In numerical models, ECS is defined as the equilibrium temperature approached after an instantaneous doubling of CO_2. Meehl et al. (2020) provide a detailed review of the concept of ECS. In the real atmosphere, instantaneous doubling of CO_2 does not occur and hence the challenge of determining the future magnitude of tropospheric global warming from current observations. In the troposphere, CO_2 continues to increase monotonically while the energy balance and temperature remain out of equilibrium (Loeb et al., 2021). The tropospheric energy imbalance is due to the time scale of the lower atmosphere climate system to adjust to radiative perturbations associated with increasing CO_2, for the various cloud, water vapor, and lapse rate feedbacks to occur, and for the ocean heat storage to come into equilibrium with the atmosphere.

In contrast, the timescales for the response of the stratosphere, mesosphere, and lower thermosphere to radiative perturbations are much shorter and can be readily calculated from the infrared radiative cooling rates. Wehrbein and Leovy (1982), Kiehl and Solomon (1986), Gille and Lyjak (1986), and Mlynczak et al. (1999) compute the radiative relaxation time (τ_{rad}) of the stratosphere and lower mesosphere as the timescale for Newtonian damping, which is defined as the ratio of a change in temperature to the change in infrared cooling due to that temperature change. τ_{rad} represents the time required for the atmosphere to reach $1/e$ (36%) its radiatve response to a perturbation. Wehrbein and Leovy (1982) based their calculations on numerical model results while the other authors used data from the Limb Infrared Monitor of the Stratosphere instrument that operated as planned between October 1978 and May 1979. Mlynczak et al. (1999) also used data from instruments aboard the Upper

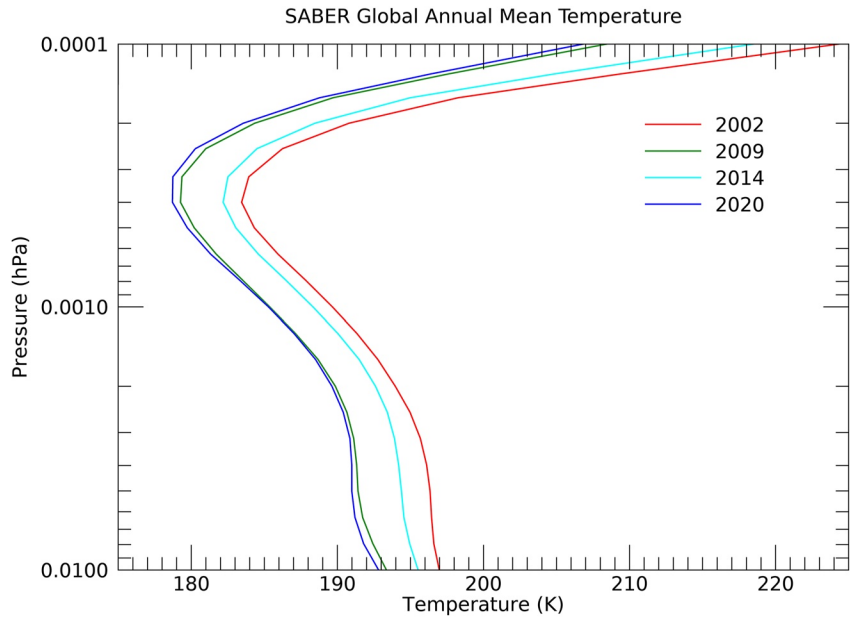

Figure 8. SABER global annual mean temperature profiles for the years 2002, 2009, 2014, and 2020. The *y*-axis ranges from 0.01 hPa (~80 km) to 0.0001 hPa (~105 km).

Atmosphere Research Satellite that was launched in 1991. They found the radiative relaxation times from 100 to 0.1 hPa (approximately 15–65 km) to range from a few months in the lower stratosphere to ~10–20 days in the lower mesosphere. These results indicate that the response of the stratosphere and lower mesosphere to thermal perturbations is prompt and there is no long-term energy storage in these regions.

Infrared radiative cooling rates are computed as part of the SABER temperature retrieval algorithm under full non-local thermodynamic equilibrium (non-LTE) using the Curtis matrix formulation, as described in Mlynczak, Hunt, et al., 2018. Radiative cooling rates for 27 different vibration-rotation bands of CO_2 are computed for each SABER temperature profile and are available as standard SABER data products. For each SABER temperature profile, we compute the total infrared cooling using the nine most significant CO_2 vibration-rotation bands.

In the upper MLT (10^{-2}–10^{-4} hPa, ~80–105 km) the radiative response is driven by the response to thermal changes and to changes in atomic oxygen because of the role of atomic oxygen in the CO_2 radiative cooling rate under conditions of non-LTE. Thermal changes (e.g., due to the solar cycle) will also be accompanied by changes in atomic oxygen, both of which influence the cooling rate under non-LTE, which is almost entirely due to infrared emission from CO_2 in the upper MLT. Using SABER global annual mean temperature data and global annual mean radiative cooling rates (due to CO_2 only), we evaluate an *equivalent* radiative relaxation rate based on the *observed* atmospheric response to temperature and atomic oxygen variations from solar maximum to solar minimum conditions. The equivalent radiative relaxation timescale τ_{eq} vertical profile is defined at each pressure level (p) is defined as in Mlynczak et al. (1999):

$$\tau_{eq}(p) = \frac{\Delta T(p)}{\Delta Q(p)} \quad (1)$$

In Equation 1, $\Delta T(p)$ is a specified change in temperature and $\Delta Q\,(p)$ is the corresponding change in the *observed* infrared radiative cooling rate, rather than a *computed* change in radiative cooling solely due to a temperature perturbation. We use the SABER global annual mean $T(p)$ and $Q(p)$ for 2002, 2009, 2014, and 2020. These are shown in Figures 8 and 9. $\Delta T(p)$ and $\Delta Q(p)$ are evaluated by taking the difference in T(p) and in Q(p) between 2002 and 2009, 2009 and 2014, and 2002 and 2020, representing differences between three different solar maxima and minima. τ_{eq} is evaluated with the corresponding ratios.

Figure 10 shows τ_{eq} for the three cases and their average. The calculated τ_{eq} decreases from approximately 8 days near 0.01 hPa to just over 1 day at 0.0001 hPa (105 km). These values of τ_{eq} are smaller than the ~7 days radiative

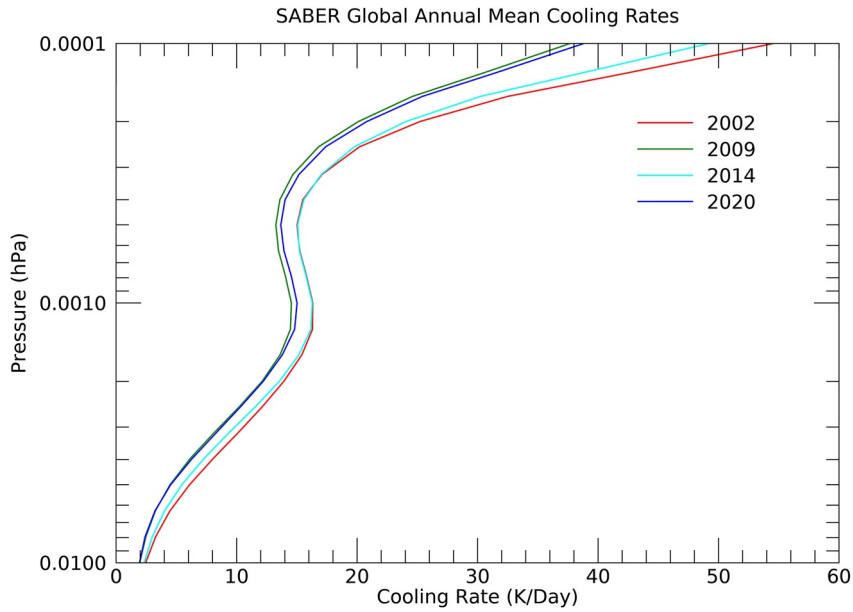

Figure 9. SABER global annual mean radiative cooling rate profiles due to CO_2 for the years 2002, 2009, 2014, and 2020. The *y*-axis ranges from 0.01 hPa (~80 km) to 0.0001 hPa (~105 km).

relaxation lifetimes of Wehrbein and Leovy (1982) at 95 km. The differences may reflect the influence of atomic oxygen on the radiative relaxation which were not well-known or considered by Wehrbein and Leovy (1982). The small values of τ_{eq} further indicate that the upper MLT will adjust promptly to additions of CO_2 and that there are no slow feedbacks or long-term energy storage.

Proceeding from this result, we expect that the rate of change in temperature associated with changing CO_2 (which we call here $\partial T/\partial q$) will be approximately constant over time or, equivalently, proportional to the rate of CO_2 increase. From this, we can develop an estimate of the sensitivity of the MLT temperature (henceforth S_{MLT}) to a doubling of CO_2 using the SABER-observed temperature trends and the SABER-established result that the growth rate of CO_2 in the MLT tracks that at the Earth's surface. We begin by defining S_{MLT} as:

$$S_{MLT} = \frac{\partial T}{\partial q}\Delta q \tag{2}$$

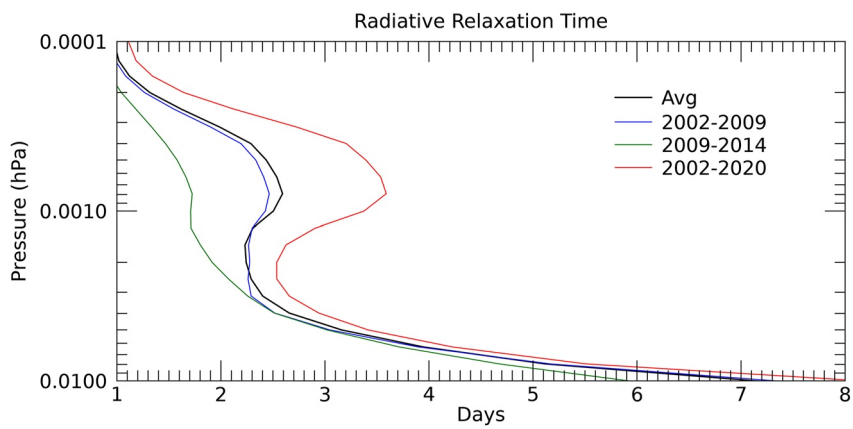

Figure 10. Calculated equivalent radiative relaxation time (days) for the upper mesosphere and lower thermosphere based on Equation 1 using global annual means cooling rates shown in Figures 6 and 7 for the years indicated in the figure. The curve "Avg"is the average of the three curves.

where $\partial T/\partial q$ is the rate of change of mesospheric/lower thermosphere temperature with respect to the rate of change of mesospheric/lower thermosphere CO_2 and Δq is the absolute change in the amount of mesospheric/lower thermosphere CO_2 when doubled. The $\partial T/\partial q$ term is estimated from the observed trends in temperature and CO_2 from SABER by assuming the relation:

$$\frac{\partial T}{\partial q} \cong \frac{\partial T}{\partial t} \div \frac{\partial q_{\mathrm{cm}}}{\partial t} \tag{3}$$

In Equation 3, ∂T/∂t is the SABER-derived trend in temperature due to increasing CO_2 (Table 1) between 1 and 10^{-3} hPa ranging between −0.51 and −0.63 K/decade. At 10^{-4} hPa, approximately 105 km, the derived trend is −2.60 K/decade. The trend ($\partial q_{\mathrm{cm}}/\partial t$) in current mesospheric CO_2, q_{cm}, in percentage terms, is approximately the same as at the surface, currently about 5% per decade at current CO_2 levels (Rezac et al., 2018). Therefore, $\partial q_{\mathrm{cm}}/\partial$t is approximately $0.05 \times q_{\mathrm{cm}}$, (units of ppm per decade). Thus, we can write using Equation 1

$$S_{\mathrm{MLT}} \cong \left\{ \frac{\partial T}{\partial t} \div \frac{\partial q_{\mathrm{cm}}}{\partial t} \right\} \times \Delta q \tag{4}$$

The last term to define is Δq, the absolute change in CO_2 due to a doubling of CO_2 from pre-industrial times. Define q_{mpi} as the CO_2 concentration in the pre-industrial mesosphere. Its doubled value is simply $2q_{\mathrm{mpi}}$. The difference, Δq is simply ($2q_{\mathrm{mpi}}$–q_{mpi}) or $\Delta q = q_{\mathrm{mpi}}$. Noting that to date, CO_2 at Earth's surface has increased approximately 50% from pre-industrial levels, the CO_2 concentration in the current mesosphere, q_{cm} is then $1.5 \times q_{\mathrm{mpi}}$ because the mesospheric CO_2 growth rate track that at the surface. Thus, $q_{\mathrm{mpi}} = q_{\mathrm{cm}}/1.5$ and since $\Delta q = q_{\mathrm{mpi}}$, Δq also equals $q_{\mathrm{cm}}/1.5$.

Using these relationships, Equation 4 can be rewritten as:

$$S_{\mathrm{MLT}} \sim \left\{ \frac{\partial T}{\partial t} \times \frac{1}{0.05 \times q_{\mathrm{cm}}} \right\} \times \frac{q_{\mathrm{cm}}}{1.5} \tag{5}$$

In Equation 5 the q_{cm} terms cancel and the S_{MLT} is then dependent only on the observed mesospheric temperature trend (∂T/∂t), the observed rate of mesospheric CO_2 increase (5% per decade) and the observed fraction (1.5 or 50%) by which mesospheric CO_2 has changed since pre-industrial times. The range of S_{MLT} based on the observed range of temperature trend in the mesosphere is found to be −6.8 K to −8.4 K (for an average of −7.5 K) at pressures greater than 10^{-3} hPa. That is, all else being equal, a doubling of CO_2 at Earth's surface, which leads to a doubling of CO_2 in the mesosphere, will cool the mesosphere by 6.8–8.4 K. This agrees well with the prediction made by Roble and Dickinson (1989) whose Figure 2 shows the doubling of CO_2 cools the MLT by 7–12 K. However, at the 10^{-4} hPa surface, the trend of −2.6 K/decade yields a value of S_{MLT} of 35 K, a value that Roble and Dickinson show would only occur above 200 km. This result suggests that the derived trends in temperature at 10^{-4} hPa associated with CO_2 increase are very likely too large. We suggest the following two reasons for this: (a) the challenge in deriving a small trend on top of a large solar cycle signal or (b) that F10.7 is not a suitable proxy for solar variability at 10^{-4} hPa. The latter possibility will be discussed in Section 5. Based on the average S_{MLT} at pressures greater than 10^{-3} hPa, we estimate that the mesosphere has cooled by approximately 3.75 K since the start of the Industrial Age due to increased CO_2.

5. Discussion of Uncertainties in SABER Temperature Data

The potential sources of uncertainty that may affect SABER temperatures (and hence, GPH and thickness) include measurement error in the form of random and systematic error uncertainties in the SABER radiance measurements, in the algorithm used to derive temperature, and possible long-term drift of instrument calibration. The uncertainties in SABER temperature data are extensively discussed in Mertens et al. (2001), Remsberg et al. (2008), and Garcia-Comas et al. (2008), hereafter collectively referred to as "MRG." Mlynczak et al. (2020) showed that the stability of the SABER calibration was between −0.1 K/decade and −0.2 K/decade in global average stratospheric temperature between 55°N and 55°S, the same latitude range as in this current paper. That is, if SABER was observing a constant temperature over time, the drift in instrument calibration would induce a false negative trend as large as 0.1–0.2 K/decade. Given that SABER was designed and built beginning over 25 years ago for a nominal 2-year mission, the demonstrated stability is remarkable, although it is a non-negligible

fraction of the observed trend in temperature in the middle atmosphere. Because the stability represents a very slow change in *calibration*, the stability at all pressure levels would be expected to follow that derived for the stratosphere. Based on the results presented in this paper, we conclude calibration stability is not the cause of the observed changes and trends in temperature, GPH, and thickness presented in this paper. The results do point out the importance of instrument calibration for all future instruments that will succeed SABER. In addition, temperature uncertainty due to random errors in SABER radiances discussed in MRG are insignificant in the highly averaged results presented here.

SABER temperatures are derived from measurements of infrared emission from the vibration-rotation bands of CO_2 in the 15 μm spectral region. In the upper MLT these bands are well-known to depart from LTE. The fundamental band of the bending mode dominates the measured emission above about 80 km. Collisions between CO_2 and atomic oxygen are critically important in determining the degree of non-LTE in the fundamental band. Therefore, the atomic oxygen concentration and the rate coefficient for collisional quenching of the first vibrational state of the bending mode of CO_2 are critical parameters in the non-LTE model. The CO_2 concentration is also a critical parameter in the retrieval of temperature, and as discussed above, is provided by the WACCM model. MRG extensively review the sensitivity of retrieved temperatures to these parameters.

The rate coefficient for O-$CO_2(\upsilon_2)$ quenching used in the SABER operational retrievals is taken from Sharma and Wintersteiner (1990). As this rate coefficient is fixed in the SABER retrieval, the only uncertainty expected to enter into the trend analysis is through errors in temperature causing errors in the rate coefficient via the temperature sensitivity of the coefficient. It is straightforward to show using Equation 1 of Sharma and Wintersteiner (1990) that a 25 K *error* in temperature results in a 12% error in the rate coefficient. We therefore discount the rate coefficient uncertainty as a source of the observed temperature, GPH, and thickness trends.

MRG have shown that errors in the CO_2 concentration and the atomic oxygen concentration can have a marked effect on the retrieved temperatures. In the SABER Version 2.07 and 2.08 temperature data used in this study, CO_2 and atomic oxygen concentrations are provided by numerical models above 90–95 km. The CO_2 data are monthly means from the NCAR WACCM and are updated for the observed growth in the CO_2 concentration. The atomic oxygen is taken from the MSIS 2000 model (Picone et al., 2002) and is largely determined by the F10.7 index. As shown in Figure 5, F10.7 varies with the solar cycle, is approximately the same during both solar minima, and visually exhibits no long-term trend. There is a trend in the CO_2 in the WACCM model that mimics the observed trend of CO_2 in the atmosphere. We therefore conclude that the observed trends in temperature are not associated with trends in the atomic oxygen or CO_2 concentrations used in the non-LTE calculations in the SABER temperature retrieval algorithm.

The derived temperature trend at 10^{-4} hPa is substantially larger than at the other four pressure levels and appears to be non-physical based on the large value that it implies for S_{MLT}. There are two probable causes for this large trend not related to the SABER retrieval algorithm. First, if the cooler temperatures in the 2019 minimum are due to a reduction in solar irradiance in the 175–200 nm region from the 2009-2009, as indicated in Woods et al., 2022, F10.7 does not appear to pick this up. If so, the use of F10.7 as a proxy for solar irradiance would not pick up the solar variability, and hence a larger temperature trend would be derived. We carried out experiments with a synthetic irradiance proxy that did show a decrease in irradiance in 2019 relative to 2008–2009 and the calculated trend at 10^{-4} hPa was reduced by as much as one-half. A second cause of the large trend is the relatively small magnitude of the trend in temperature due to CO_2 increase relative to the magnitude of the change due to the variability of the solar cycle. The size of the natural variability relative to the size of the trend may require a longer data set, more accurate solar proxies, and more accurate temperature data for MLR to accurately derive the trend.

Finally, we note that an error in SABER temperatures above ~85 km due to a non-physical trend in CO_2 from 2020 onward was discovered and corrected in mid-2022. The WACCM CO_2 provided to the SABER temperature algorithm from 2020 onward was taken from a different version of the model than had been used through 2019. This new version had a larger CO_2 concentration above 85 km than the other version, by as much as 15%. Consequently, a large cooling trend was induced in the SABER temperature record, particularly above 90–95 km, from 2020 onward. Upon discovering this (in early summer, 2022), the entire SABER data set was reprocessed from 2020 onward with the version of WACCM that is consistent with all prior years. The temperature data presented in this paper are the reprocessed and consistent temperatures from 2002 onward. The SABER team is preparing a

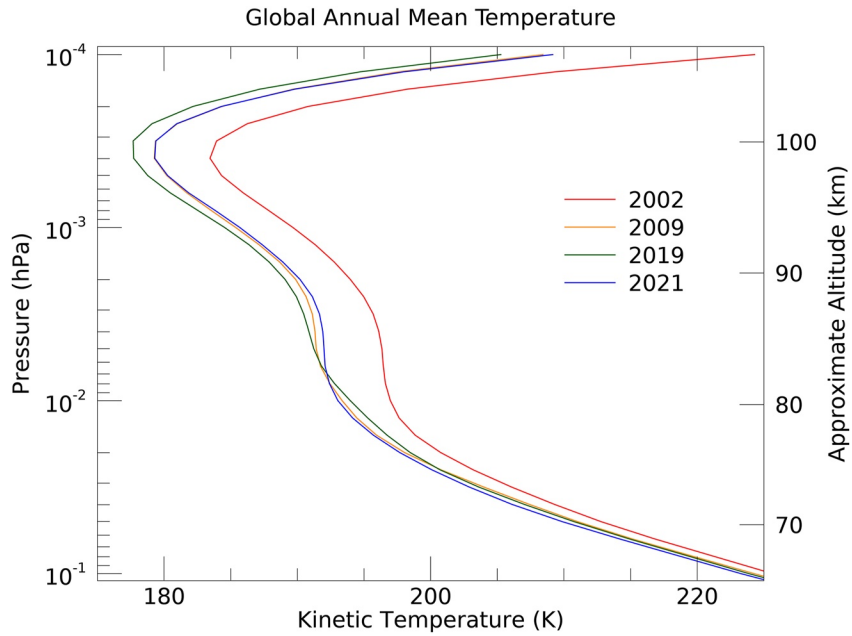

Figure 11. SABER global annual mean temperature profiles for years 2002, 2009, 2019, and 2021. See text for discussion.

separate paper on the topic of algorithm instability in long-term data records to highlight the importance of stable algorithms in detecting long-term changes. The SABER data from 2020 onward is referred to as version 2.08.

6. Summary

CO_2 has been increasing in Earth's atmosphere due to the combustion of fossil fuels since the beginning of the Industrial Age. The increase of CO_2 has been predicted to alter the thermal structure of the atmosphere from Earth's surface to the edge of Space. In this paper, we have shown the combined effects of increasing CO_2 and declining solar activity on the temperature and thickness of the MLT over the 20-year period from 2002 to 2021 that included two deep solar minima.

Bailey et al. (2021) have noted that "With regard to the geometric heights of mesospheric pressure levels, model studies (Akmaev et al., 2006; Lübken et al., 2009, 2013; Lübken & Berger, 2011) indicate a shrinking of the height of the mesosphere attributed to greenhouse gas cooling. This contraction lowers the height of mesospheric pressure levels and leads to cooling just below the heights of polar mesospheric cloud heights and warming just above (e.g., Lübken & Berger, 2011; Lübken et al., 2013.) Bailey et al. (2021) further comment that they know of no observational studies to date of trends in mesospheric pressure heights, but Friedrich et al. (2017) have suggested such trends based on studies of observed D and E-region electron densities. The SABER GPH results presented here document for the first time the contraction of the near-global MLT since 2002.

The SABER data and consideration of solar activity and the growth of CO_2 since the late 1700's strongly suggest that the MLT during the recent two solar minima are the coldest since the onset of the Industrial Age. Figure 11 shows the global annual mean temperatures for 2002, the solar minima years of 2009 and 2019, and the most recent complete year, 2021. The years 2009, 2019, and 2021 are all colder than 2002 throughout the MLT over the indicated pressure range. The year 2019 is colder than all other years for pressures less than 0.007 hPa. 2009 is slightly cooler than 2019 between the pressures of 0.007 and 0.025 hPa, and they are essentially identical between 0.025 and 0.1 hPa. The year 2021 is very slightly cooler than 2009 and 2019 at pressures greater than 0.007 hPa. These results reinforce the concept that the current and most recent solar minima time periods very likely correspond to the coldest conditions in the MLT since the start of the Industrial Age. In addition, consideration of the rapid temporal response of the MLT to radiative perturbations leads to the derivation of the sensitivity of the MLT to a doubling of CO_2 to be −7.5 K. As the CO_2 concentration is currently about halfway to doubling since pre-industrial times, we conclude that the MLT has cooled by about −3.75 K since the mid-1700's.

A detailed consideration of the uncertainties in SABER temperatures leads to the conclusion that various errors in the temperature retrieval process are not responsible for the derived trends in *T*, GPH, and thickness. The seemingly too-large trend at 10^{-4} hPa may be due to a decrease in solar irradiance not captured by the F10.7 proxy used in the MLR trend determination. In addition, the small magnitude of the trend relative to the magnitude of the solar variability likely requires both a longer data record and a more accurate solar proxy to enable accurate trend detection at that pressure level.

The possibility that a reduction in solar irradiance in the Schumann-Runge band spectral region (175–200 nm) that is not characterized by the F10.7 index but is responsible for colder temperatures at 10^{-4} hPa in 2019 than in 2009 raises a broader question about solar irradiance proxies used in multiple linear regressions. F10.7 is a monochromatic index representing the variability of solar irradiance at 10.7 cm and whose time series dates from 1947. It is widely used as a proxy representing many facets of solar variability because of its longevity and availability. However, in the upper MLT, solar heating occurs through absorption of ultraviolet radiation at Ly-α wavelength (121.5 nm), in the SRC (130–175 nm), and in the SRB (175–200 nm). Over a solar cycle the solar irradiance varies substantially *with wavelength* across the 121–200 nm interval. In addition, the molecular oxygen absorption cross sections in the SRB are temperature dependent, adding an additional *wavelength-dependent* solar-cycle dependence to the solar heating. Furthermore, substantial heating is accomplished by exothermic chemical reactions which are the by-products of the solar photolysis of O_2 and H_2O in the ultraviolet. These reactions are liberating large amounts of solar energy, often long after and far away from the location of the photolysis event (Mlynczak & Solomon, 1993). It would indeed be surprising if a single, monochromatic index (i.e., F10.7) adequately represented the effects of solar variability on the thermal structure of the upper MLT. It seems very likely that multiple solar proxies, perhaps the ultraviolet solar irradiances themselves, should be used in multiple linear regressions in place of F10.7. We plan to examine this possibility in more detail in the near future.

Understanding the long-term evolution of the temperature and density of the MLT is much more than a scientific interest. Mlynczak, Yue et al. (2021) discuss potential consequences for the habitability of the space environment due to increasing CO_2 and subsequent cooling in the MLT. The associated cooling and contraction of geospace results in less aerodynamic drag on space vehicles—and on space debris. Already a problem, increasing and longer-lived space debris pose a potential threat to habitability of space and frequently used orbital planes. It seems likely that ongoing changes in space climate will become important issues in space law, space policy, and in the business of underwriting insurance for endeavors in space. Continued observations of the MLT in addition to those of the lower atmosphere and the geospace environment are essential to verify, understand, and ultimately mitigate multiple ongoing changes to the entire atmosphere and their likely impacts on the global and space economies.

Data Availability Statement

All SABER data used in this paper is available from the SABER project data server at http://saber.gats-inc.com/data_services.php (Remsberg et al., 2008; Garcia-Comas et al., 2008). The ice core CO_2 data in Figure 6 is obtained from: https://www.ncei.noaa.gov/pub/data/paleo/contributions_by_author/frank2010/smoothedco2.txt (Frank et al., 2010). The F10.7 Solar Radio Flux data are obtained daily from the National Space Weather Prediction Center. Users can get the historic data from: ftp://ftp.swpc.noaa.gov//pub/indices/old_indices. Note that most popular web browsers and some computer operating systems have dropped built-in support for the FTP protocol. A separate FTP client should be used instead. Additional data analyses were done using ENVI version 4.8 (Exelis Visual Information Solutions, Boulder, Colorado).

Acknowledgments
MGM and LAH acknowledge support under the NASA TIMED/SABER Project and the NASA Heliophysics Supporting Research program. JY was supported by NSF AGS-1901126 and the NASA Aeronomy of Ice in the Mesosphere (AIM) missions. JY acknowledges the assistance of N. Wang in plotting data in Figure 6. VLH acknowledges support from the AIM mission. AIM is funded by the NASA Small Explorer program.

References

Akmaev, R. A., Fomichev, V. I., & Zhu, X. (2006). Impact of middle-atmospheric composition changes on greenhouse cooling in the upper atmosphere. *Journal of Atmospheric and Solar-Terrestrial Physics*, *68*(17), 1879–1889. https://doi.org/10.1016/j.jastp.2006.03.008

Bailey, S. M., Thurairajah, B., Hervig, M. E., Siskind, D. E., Russell, J. M., III, & Gordley, L. L. (2021). Trends in polar summer mesosphere temperatures and pressure altitude from satellite observations. *Journal of Atmospheric and Solar-Terrestrial Physics*, *220*, 105650. https://doi.org/10.1016/j.jastp.2021.105650

Bates, D. R. (1951). The temperature of the upper atmosphere. *Proceedings of the Physical Society Section B*, *64*(9), 805–821. https://doi.org/10.1088/0370-1301/64/9/312

Cicerone, R. J. (1990). Greenhouse cooling up high. *Nature*, *344*(6262), 104–105. https://doi.org/10.1038/344104a0

Coddington, J. L., Lean, P., Pilewskie, M. S., & Lindholm, D. (2016). A solar irradiance climate data record. *Bulletin of the American Meteorological Society*, *97*(7), 1265–1282. https://doi.org/10.1175/BAMS-D-14-00265.1

Curtis, A. R., & Goody, R. M. (1956). Thermal radiation in the upper atmosphere. *Proceedings of the Royal Society of London A*, *236*. https://www.jstor.org/stable/100028

Dickinson, R. E. (1984). Infrared cooling in the mesosphere and lower thermosphere. *Journal of Atmospheric and Solar-Terrestrial Physics*, *46*(11), 995–1008. https://doi.org/10.1016/0021-9169(84)90006-0

Emmert, J. A. (2015). Thermospheric mass density: A review. *Advances in Space Research*, *56*(5), 773–824. https://doi.org/10.1016/j.asr.2015.05.038

Frank, D. C., Esper, J., Raible, C. C., Büntgen, U., Trouet, V., Stocker, B., & Joos, F. (2010). Ensemble reconstruction constraints on the global carbon cycle sensitivity to climate [Dataset]. Nature, *463*(7280), 527–532. https://doi.org/10.1038/nature08769

Friedrich, M., Pock, C., & Torkar, K. (2017). Long-term trends in the D- and E-region based on rocket-borne measurements. *Journal of Atmospheric and Solar-Terrestrial Physics*, *163*, 78–84. https://doi.org/10.1016/j.jastp.2017.04.009

García-Comas, M., Lopez-Puertas, M., Marshall, B. T., Wintersteiner, P. P., Funke, B., Bermejo-Pantaleon, D., et al. (2008). Errors in Sounding of the Atmosphere using Broadband Emission Radiometry (SABER) kinetic temperature caused by non-local-thermodynamic-equilibrium model parameters. [Dataset]. Journal of Geophysical Research, *113*(D24), D24106. https://doi.org/10.1029/2008JD010105

Garcia, R. R., Yue, J., & Russell, J. M., III. (2019). Middle atmosphere temperature trends in the twentieth and twenty-first centuries simulated with the Whole Atmosphere Community Climate Model (WACCM). *Journal of Geophysical Research: Space Physics*, *124*(10), 7984–7993. https://doi.org/10.1029/2019JA026909

Gettelman, A., Mills, M. J., Kinnison, D. E., Garcia, R. R., Smith, A. K., Marsh, D. R., et al. (2019). The whole atmosphere community climate model version 6 (WACCM6). *Journal of Geophysical Research: Atmospheres*, *124*(23), 12380–12403. https://doi.org/10.1029/2019JD030943

Gille, J. C., & Lyjak, L. V. (1986). Radiative heating and cooling rates in the middle atmosphere. *Journal of the Atmospheric Sciences*, *43*(20), 2215–2229. https://doi.org/10.1175/1520-0469(1986)043<2215:RHACRI>2.0.CO;2

Kiehl, J. T., & Solomon, S. (1986). The radiative balance of the stratosphere. *Journal of the Atmospheric Sciences*, *43*(14), 1525–1534. https://doi.org/10.1175/1520-0469(1986)043<1525:OTRBOT>2.0.CO;2

Kockarts, G. (1980). Nitric oxide cooling in the terrestrial thermosphere. *Geophysical Research Letters*, *7*(2), 137–140. https://doi.org/10.1029/GL007i002p00137

Kuhn, W. R., & London, J. (1969). Infrared radiative cooling in the middle atmosphere. *Journal of the Atmospheric Sciences*, *26*(2), 189–204. https://doi.org/10.1175/1520-0469(1969)026<0189:IRCITM>2.0.CO;2

Loeb, N. G., Johnson, G. C., Thorsen, T. J., Lyman, J. M., Rose, F. G., & Kato, S. (2021). Satellite and ocean data reveal marked increase in Earth's heating rate. *Geophysical Research Letters*, *48*(13), e2021GL093047. https://doi.org/10.1029/2021GL093047

London, J. (1980). Radiative energy sources and sinks in the stratosphere and mesosphere. *Proceedings of the NATO Advanced Study Institute* (pp. 703–721).

Lübken, F.-J., & Berger, U. (2011). Latitudinal and interhemispheric variation of stratospheric effects on mesospheric ice layer trends. *Journal of Geophysical Research*, *116*, D00P03. https://doi.org/10.1029/2010JD015258

Lübken, F.-J., Berger, U., & Baumgarten, G. (2009). Stratospheric and solar cycle effects on long-term variability of mesospheric ice clouds. *Journal of Geophysical Research*, *114*(D1), D00106. https://doi.org/10.1029/2009JD012377

Lübken, F.-J., Berger, U., & Baumgarten, G. (2013). Temperature trends in the midlatitude summer mesosphere. *Journal of Geophysical Research: Atmospheres*, *118*(24), 13347–13360. https://doi.org/10.1002/2013JD020576

Meehl, G. A., Senior, C. A., Eyring, V., Flato, G., Lamarque, J.-F., Stouffer, R. J., et al. (2020). Context for interpreting equilibrium climate sensitivity and transient climate response from the CMIP6 Earth system models. *Science Advances*, *6*(26), eaba1981. https://doi.org/10.1126/sciadv.aba1981

Mertens, C. J., Mlynczak, M. G., Garcia, R. R., & Portmann, R. W. (1999). A detailed evaluation of the stratospheric heat budget: 1. Radiation transfer. *Journal of Geophysical Research*, *104*(D6), 6021–6038. https://doi.org/10.1029/1998JD200100

Mertens, C. J., Mlynczak, M. G., López-Puertas, M., Wintersteiner, P. P., Picard, R. H., Winick, J. R., et al. (2001). Retrieval of mesospheric and lower thermospheric kinetic temperature from measurements of CO_2 15 μm Earth Limb Emission under non-LTE conditions. *Geophysical Research Letters*, *28*(7), 1391–1394. https://doi.org/10.1029/2000GL012189

Mlynczak, M. G., Daniels, T., Hunt, L. A., Yue, J., Marshall, B. T., Russell, J. M., et al. (2020). Radiometric stability of the SABER instrument. *Earth and Space Science*, *7*(2), e2019EA001011. https://doi.org/10.1029/2019EA001011

Mlynczak, M. G., Hunt, L. A., Lopez-Puertas, M., Funke, B., Emmert, J., Solomon, S., et al. (2021). Spectroscopy, gas kinetics, and opacity of thermospheric nitric oxide and implications for analysis of SABER infrared emission measurements at 5.3 μm. *Journal of Quantitative Spectroscopy and Radiative Transfer*, *268*, 107609. https://doi.org/10.1016/j.jqsrt.2021.107609

Mlynczak, M. G., Hunt, L. A., Russell, J. M., & Marshall, B. T. (2018). Updated SABER night atomic oxygen and implications for SABER ozone and atomic hydrogen. *Geophysical Research Letters*, *45*(11), 5735–5741. https://doi.org/10.1029/2018GL077377

Mlynczak, M. G., Hunt, L. A., Thomas Marshall, B., Martin-Torres, F. J., Mertens, C. J., Russell, J. M., et al. (2010). Observations of infrared radiative cooling in the thermosphere on daily to multiyear timescales from the TIMED/SABER instrument. *Journal of Geophysical Research*, *115*(A3), A03309. https://doi.org/10.1029/2009JA014713

Mlynczak, M. G., Knipp, D. J., Hunt, L. A., Gaebler, J., Matsuo, T., Kilcommons, L. M., & Young, C. L. (2018). Space-based sentinels for measurement of infrared cooling in the thermosphere for space weather nowcasting and forecasting. *Space Weather*, *16*(4), 363–375. https://doi.org/10.1002/2017SW001757

Mlynczak, M. G., Mertens, C. J., Garcia, R. R., & Portmann, R. W. (1999). A detailed evaluation of the stratospheric heat budget: 2. Global radiation balance and diabatic circulations. *Journal of Geophysical Research*, *104*(D6), 6039–6066. https://doi.org/10.1029/1998JD200099

Mlynczak, M. G., & Solomon, S. (1993). A detailed evaluation of the heating efficiency in the middle atmosphere. *Journal of Geophysical Research*, *98*(D6), 10517–10541. https://doi.org/10.1029/93JD00315

Mlynczak, M. G., Yue, J., McCormack, J., Liebermann, R. S., & Livesey, N. J. (2021). An observational gap at the edge of space. *Eos*, *102*. https://doi.org/10.1029/2021EO155494

National Research Council. (1979). *Carbon dioxide and climate: A scientific assessment*. The National Academies Press. https://doi.org/10.17226/12181

Nicholls, N. (2019). The Charney report: 40 years ago, scientists accurately predicted climate change. Retrieved from https://phys.org/news/2019-07-charney-years-scientists-accurately-climate.html

Picone, J. M., Hedin, A. E., Drob, D. P., & Aikin, A. C. (2002). NRLMSISE-00 empirical model of the atmosphere: Statistical comparisons and scientific issues. *Journal of Geophysical Research*, *107*(A12), 1468. https://doi.org/10.1029/2002JA009430

Pisoft, P., Sacha, P., Polvani, L. M., Anel, J. A., de la Torre, L., Eichinger, R., et al. (2021). Stratospheric contraction caused by increasing greenhouse gases. *Environmental Research Letters*, *16*(6), 064038. https://doi.org/10.1088/1748-9326/abfe2b

Randel, W. J., Polvani, L., Wu, F., Kinnison, D. E., Zou, C.-Z., & Mears, C. (2017). Troposphere-stratosphere temperature trends derived from satellite data compared with ensemble simulations from WACCM. *Journal of Geophysical Research: Atmospheres*, *122*(18), 9651–9667. https://doi.org/10.1002/2017JD027158

Remsberg, E. E., Marshall, B. T., Garcia-Comas, M., Krueger, D., Lingenfelser, G. S., Martin-Torres, J., et al., (2008). Assessment of the quality of the Version 1.07 temperature-versus-pressure profiles of the middle atmosphere from TIMED/SABER. [Dataset]. Journal of Geophysical Research, *113*(D17), D17101. https://doi.org/10.1029/2008JD010013

Rezac, L., Yue, J., Yongxiao, J., Russell, J. M., III, Garcia, R., Lopez-Puertas, M., & Mlynczak, M. G. (2018). On long-term SABER CO_2 trends and effects due to nonuniform space and time sampling. *Journal of Geophysical Research: Space Physics*, *123*(9), 7958–7967. https://doi.org/10.1029/2018JA025892

Roble, R. G., & Dickinson, R. E. (1989). How will changes in carbon dioxide and methane modify the mean structure of the mesosphere and thermosphere? *Geophysical Research Letters*, *16*(12), 1441–1444. https://doi.org/10.1029/GL016i012p01441

Sawyer, J. S. (1972). Man-made carbon dioxide and the "greenhouse" effect. *Nature*, *239*(5366), 23–26. https://doi.org/10.1038/239023a0

Sharma, R. P., & Wintersteiner, P. P. (1990). Role of carbon dioxide in cooling planetary atmospheres. *Geophysical Research Letters*, *17*(12), 2201–2204. https://doi.org/10.1029/GL017i012p02201

Sherwood, S. C., Webb, M. J., Annan, J. D., Armour, K. C., Forster, P. M., Hargreaves, J. C., et al. (2020). An assessment of Earth's climate sensitivity using multiple lines of evidence. *Reviews of Geophysics*, *58*(4), e2019RG000678. https://doi.org/10.1029/2019RG000678

Wehrbein, W. M., & Leovy, C. B. (1982). An accurate radiative heating and cooling algorithm for use in a dynamical model of the middle atmosphere. *Journal of the Atmospheric Sciences*, *39*(7), 1532–1544. https://doi.org/10.1175/1520-0469(1982)039<1532:AARHAC>2.0.CO;2

Woods, T. N., Eparvier, F. G., Bailey, S. M., Chamberlin, P. C., Lean, J., Rottman, G. J., et al. (2005). Solar EUV Experiment (SEE): Mission overview and first results. *Journal of Geophysical Research*, *110*(A1), A01312. https://doi.org/10.1029/2004JA010765

Woods, T. N., Harder, J. W., Kopp, G., & Snow, M. (2022). Solar-cycle variability results from the solar radiation and climate experiment (SORCE) mission. *Solar Physics*, *297*(4), 43. https://doi.org/10.1007/s11207-022-01980-z

Yue, J., Russell, J., III, Jian, Y., Rezac, L., Garcia, R., López-Puertas, M., & Mlynczak, M. G. (2015). Increasing carbon dioxide concentration in the upper atmosphere observed by SABER. *Geophysical Research Letters*, *42*(17), 7194–7199. https://doi.org/10.1002/2015GL064696

Zhao, X. R., Sheng, Z., Shi, H. Q., Weng, L. B., & He, Y. (2021). Middle atmosphere temperature change derived from SABER observations 2002-20. *Journal of Climate*, *1*. https://doi.org/10.1175/JCLI-D-20-1010.1